Terahertz multispectral imaging of epitaxially grown semiconductors' lattice defects

Anis Rahman

Applied Research & Photonics, Inc.
470 Friendship Road, Suite 10
Harrisburg, PA 17111, USA Harrisburg, PA 17111, USA
*e-mail: a.rahman@arphotonics.net

Abstract – Epitaxially grown SiGe and Ge layers on Si <100> substrate have been analyzed by terahertz multispectral reconstructive 3D imaging technique. In particular, 3D images of both samples were generated via a non-contact and no-destructive route and were analyzed by utilizing the terahertz reconstructive imaging algorithm. It was found that the algorithm of "gridding with inverse distance to power equations" adopted herein for reconstructive imaging is capable of reproducing the results accurately as indicated by a good match with the TEM images of the same samples. Both the 3D and 2D images were analyzed by graphical means to determine the respective layers' thicknesses. The results were compared with the TEM images. Both the terahertz and TEM results were found to be in good agreement. Further, the imaging technique was also able to detect and quantify the size of small features of <1 nm present in the SiGe epi layer. In addition, lattice stacking fault and dislocations were also visualized and identified.

Keywords—Terahertz 3D imaging; reconstructive multispectral imaging; sub-surface analysis; non-destructive; non-contact; layer by layer; nanometer resolution.

I. INTRODUCTION

Epitaxially grown semiconductor layers involve inherent strain in their lattice structure. For some applications, the strain in the epitaxial layers of a grown semiconductor is relieved by the introduction of misfit dislocations [1]. A fully relaxed Si0.7Ge0.3 layer, for instance, is required as a buffer layer for high mobility field effect transistors having strained Si or strained SiGe channels. In this case it is necessary to control the growth conditions and the design of the structure so as to minimize the density of dislocations threading through device layers grown on top of the relaxed buffer layer. The need to prevent strain relaxation in thin layers or to control the density and distribution of defects in relaxed structures has led to extensive research on strain relaxation mechanisms and also on the properties of the defects which are required to relieve the strain. Therefore, visualization and spectroscopic characterization of these structures on a nanometer scale is of paramount importance. The spectroscopic characterization will help identify and/or detect the chemical nature of the materials while a high resolution visualization will let one quantify various features of the sample under investigation. Especially, the capability of sub-surface inspection on a layer-by-layer basis with sub-nanometer image resolution is the key for success in creating such 3D structures in a controlled fashion. Effective testing for minimized wafer rejection during process development was discussed elsewhere [2, 3]. In this report, we describe high resolution reconstructive imaging of strain relaxed SiGe/Ge/Si structures. Two cases are examined and compared. Grown Ge epitaxial layer on Si <001> substrate is inspected by 3D imaging. Also, a sample of SiGe layer grown on top of the Ge buffer of the first case was also investigated. Clear visualization of the lattice planes and their stacking fault was demonstrated. We utilize terahertz non-contact multispectral reconstructive imaging to investigate aforementioned epitaxial semiconductor layers. An algorithm of gridding with inverse distance to power equations has been used for reconstructive imaging [3]. The image is analyzed for identification of unique features and/or lattice defects. Both 2D and 3D imaging techniques are used. Additionally, graphical analysis of the images has been utilized to measure the interface features and layer thicknesses.

II. RECONSTRUCTIVE IMAGING WITH NANOMETER RESOLUTION

A detail of the multispectral reconstructive imaging technique was described elsewhere [3, 5]. Reconstructive imaging is used as an alternative for focal plane array or charged coupled device (CCD) based imaging such as those used in digital cameras. This includes electron microscopes, light microscopes and most other devices for imaging.

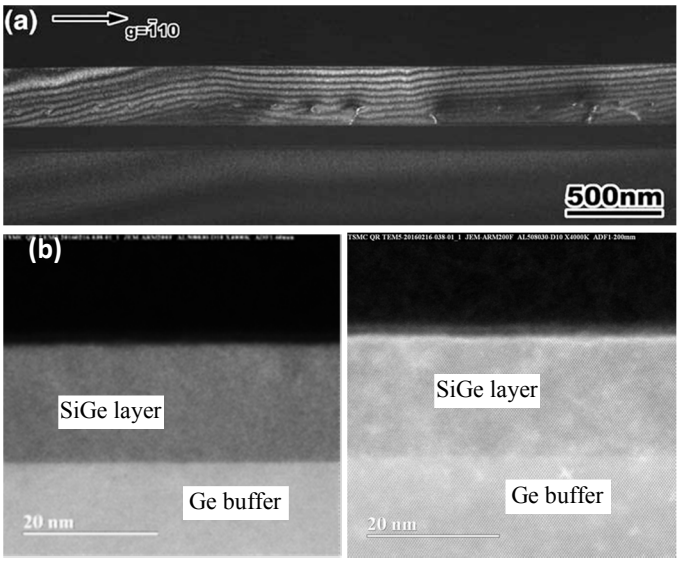

Fig. 1. (a) TEM image of stacking fault in SiGe layer [1]. (b) TEM images of sample D10 showing thicknesses of SiGe layer is ~18 nm [4].

However, in digital imaging the resolution is defined by the array elements in a CCD, for example. This limitation hinders achieving higher resolution, because, the pixel size is defined by the size of the array elements of the sensor/CCD used for image generation. Also, it is strictly a surface imaging device. TEM offers high resolution imaging; however, it is a destructive technique with stringent, time consuming sample preparation requirements. For TEM, for example, the samples must remain in high vacuum while the electron beam is accelerated by a high electric field. A TEM and SEM can measure only small samples that fit in its vacuum chamber. Atomic force microscope is also a surface imaging device for small geometry samples. Reconstructive imaging, on the other hand, offers an important opportunity to define the pixel size (or voxel size in 3D) by a hardware and software combination. Here, the response from an object is recorded on the three dimensional space as it is rasterized as shown in Fig. 2. The recoded response is then converted to 3D images via an algorithm such as gridding with inverse power law [6, 7]. The working principle is illustrated in Appendix-I.

III. Experimental Results and Discussion

Terahertz (or, T-ray) multispectral reconstructive imaging was carried out by an integrated terahertz nanoscanning time-domain spectrometer (Applied Research & Photonics, Harrisburg, PA). Samples, as received, are one of each small pieces of expitaxial wafers, cut in the form of approximately 1" by 2" rectangles, without any patterns. The first sample, composed of an epitaxial Ge buffer grown on Si<001> substrate, is termed as Sample-D02. The Ge buffer is expected to be ~600 nm thick per data provided by the supplier [4]. The second sample is termed Sample-D10, contains a SiGe layer grown on top of the Ge buffer on Si<001>, where the SiGe epitaxial layer is reported to be 18 nm as determined by TEM (see Fig. 1) [4]. The samples are mounted one at a time on the nanoscanner without any modifications. The scanning time required for terahertz multispectral data acquisition is dependent on the desired resolution of measurements. For example, at a lateral target resolution of 25 nm, the scanning is done at 500 nm/s. Thus, for scanning a surface of 2 µm × 2 µm, total elapsed time is ~320s. At a lower resolution, this time is significantly lower. The positioning system has the highest speed of ~10 mm/s. Thus, rasterizing a 200 mm wafer at 10 mm/s and at a lateral resolution of ~ 1 mm, total time needed is ~400 s. The time requirement is the same for either a plane wafer or a patterned wafer. The smallest scan able area is < 1 μm^2 and the biggest area in the current setup may be up to 300 mm × 300 mm. The measurement area may be expanded to 450 mm × 450 mm by changing the positioning system. Since, Si and other semiconductors are transparent to T-rays, the entire thickness of a blank or patterned wafer may be probed. The measurements are carried out in exact coordinates; therefore, any point within the volume of the entire wafer may be analyzed after rasterization is completed.

A stacking fault is a type of defect which characterizes the disordering of crystallographic planes. It is known as a planar defect. A stacking fault is a one or more layer interruption in the stacking sequence of atom planes. Many compound semiconductors, such as those resulting from combining elements from groups III and V or from groups II and VI of the periodic table, crystallize in the face centered cubic (FCC), zincblende or hexagonal closed pack (HCP) wurtzite crystal structures. In a semiconductor, the FCC and HCP phases of a given material will usually have different band gap energies. Consequently, when the crystal phase of a stacking fault has a lower band gap than the surrounding phase, it forms a quantum well. In the opposite case (higher band gap in the stacking fault), it constitutes an energy barrier in the band structure of the crystal that can affect the current transport in semiconductor devices [8, 9].

Dislocations are another type of defect in crystalline structures where the atoms are out of position in the lattice. Dislocations are generated and move as a result of an applied stress. The motion of dislocations allows slip – plastic deformation to occur. There are a few different kinds of dislocations in crystals such as edge dislocation and screw dislocation. In general, the dislocations act as electrical defects in optical materials and semiconductors; however, detailed discussion on the dislocations is available in text books [see for example, ref. 10] and further described in Appendix-I.

Fig. 2 exhibits the 3D rasterized data for Sample-D02. Figs. 3–7 exhibit the terahertz reconstructive images and analysis of Sample-D02. Fig. 3 shows a 1 μm^3 volume of Ge grown on Si <100>; a single face (side surface) of the cube is shown in Fig. 4. Fig. 5 shows a graphical analysis of the lattice structure of Fig. 4. The Ge buffer's thickness was determined to be ~590 nm which is in agreement with the TEM image of 600 nm [4].

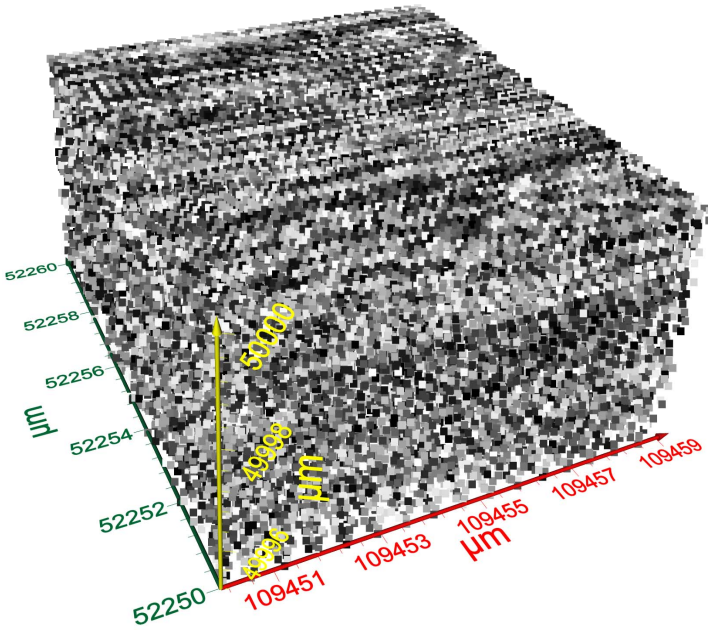

Fig. 2. Sample D02: Scatter plot of data as measured (rasterized) in X-, Y-, and Z-directions; 10 µm x 10 µm x 5 µm on a layer by layer basis.

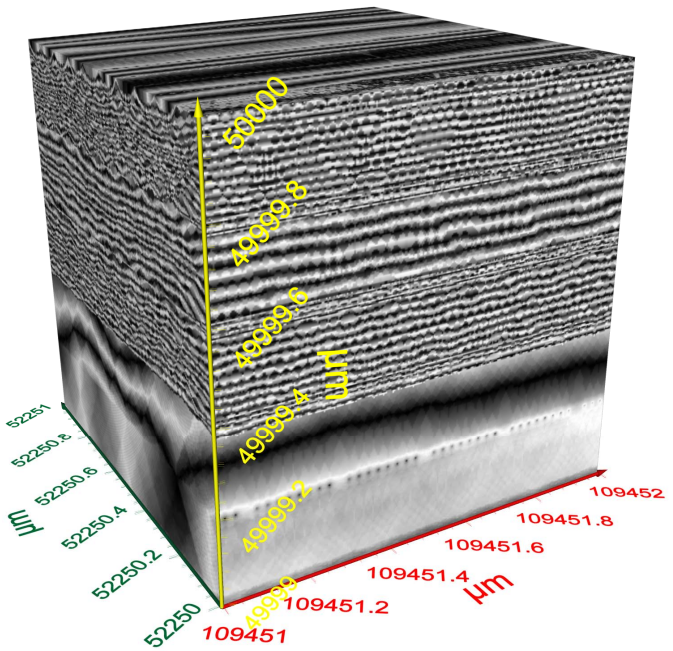

Fig. 3. Sample-D02: one cubic micron volume showing the Ge buffer's lattice structure grown on Si <100> substrate.

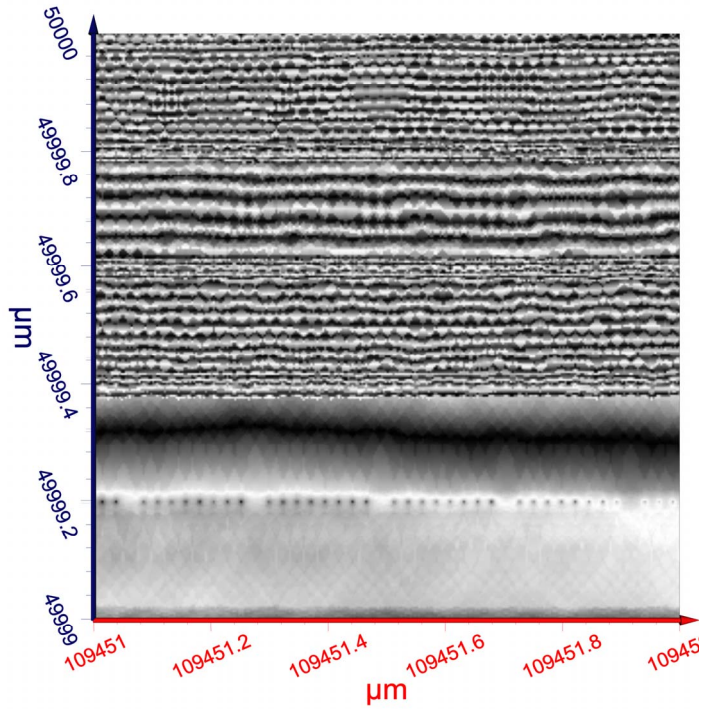

Fig. 4. Sample-D02: one square micron face (XZ surface) extracted from Fig. 3.

Fig. 6 exhibits a broader segment of Sample-D02; the top portion shows the lattice structure of Ge (~600 nm) with many stacking faults and dislocations visible. Fig. 7 shows a close up of Fig. 6 (see axis-scale). Here the stacking faults are identified the changes in the crystal lattice pattern. Edge dislocations are also visible (see arrow).

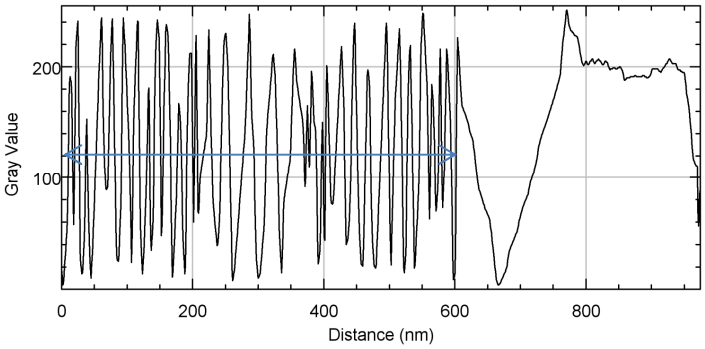

Fig. 5. Graphical analysis along the vertical line of Sample-D02, see inset of Fig. 4. Measured thickness of the Ge layer is ~ 600 nm (see arrow).

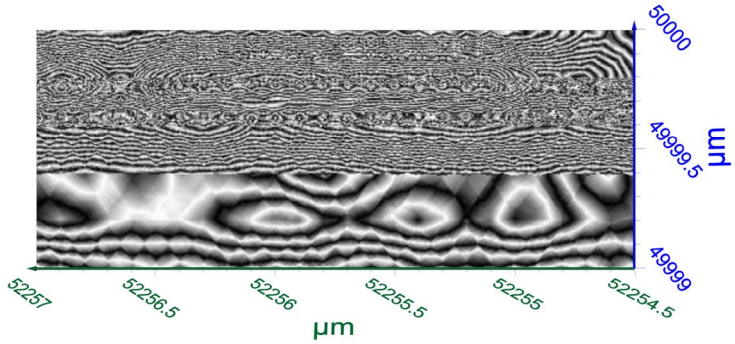

Fig. 6. A broader view of D02: 3.5 µm x 1 µm. The thickness of the Ge layer is still ~ 600 nm.

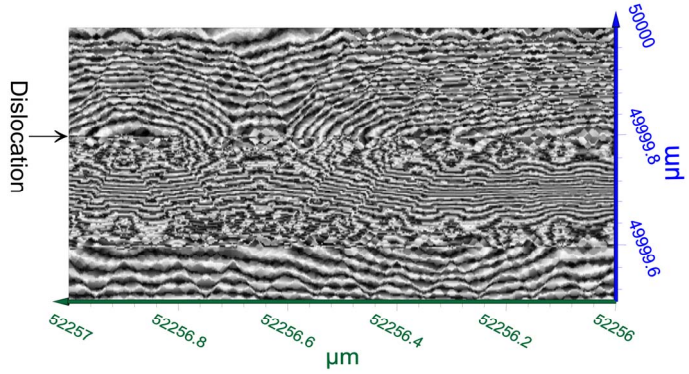

Fig. 7. A close up of Fig. 6 (see axis-scale) (1 µm × 500 nm). Changes in crystal lattice pattern indicate the stacking fault. Edge dislocations are also visible.

Fig. 8 shows 4 different slices from the volume of Fig. 3; thus exhibiting the layer by layer analysis capability. Fig. 9 shows a 1 μm^3 volume of Sample-D10 and Fig. 10 shows a slice of 500 nm^2 surface extracted from Fig. 9. A graphical analysis of the top layer of the image in Fig. 10 is shown in Fig. 11. The thickness of the SiGe (top) layer is ~18 nm; this is the same thickness as determined by TEM image, See Fig. 2.

In addition, some features of size ~1 nm were also observed in some slices of the SiGi layer. An example of such a small feature is shown in Fig. 12 by taking a single slice from Fig. 9. Fig. 13 shows a graphical analysis of a single particle of size ~0.75 nm. The origin of these nanoparticles is not clear yet; further investigation is necessary in collaboration with the manufacturer of these samples [4]. It is, however, presumed

that the small features visible in the image could be some sort of inclusions or a different phase. Thus, spectroscopic analysis and identification of these features could help adjusting the process parameters for controlling such features or inclusions. Future investigations should be designed to establish the nature and identity of this and other kind of defects.

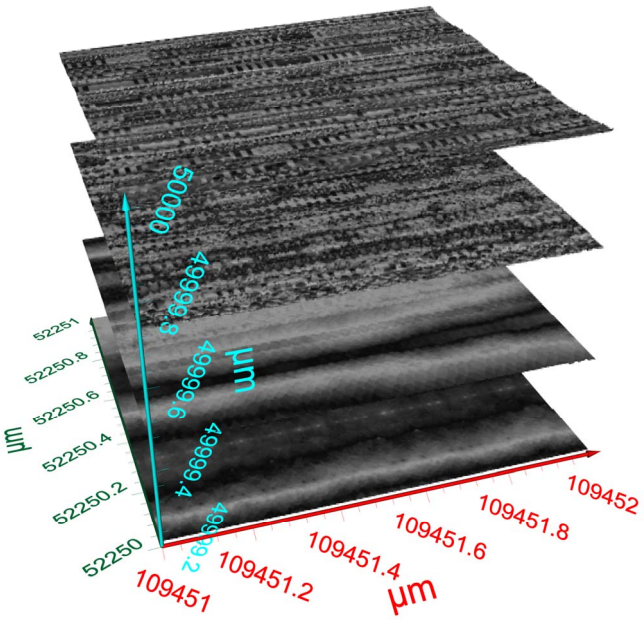

Fig. 8. A view of four different layers extracted from Fig. 3.

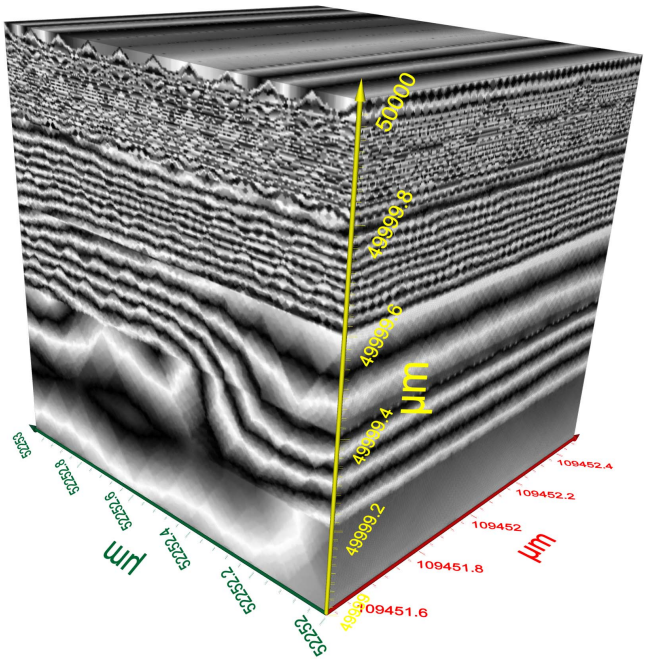

Fig. 9. Sample-D10: One cubic micron volume showing the lattice structure of Ge buffer and grown SiGe layer on the top.

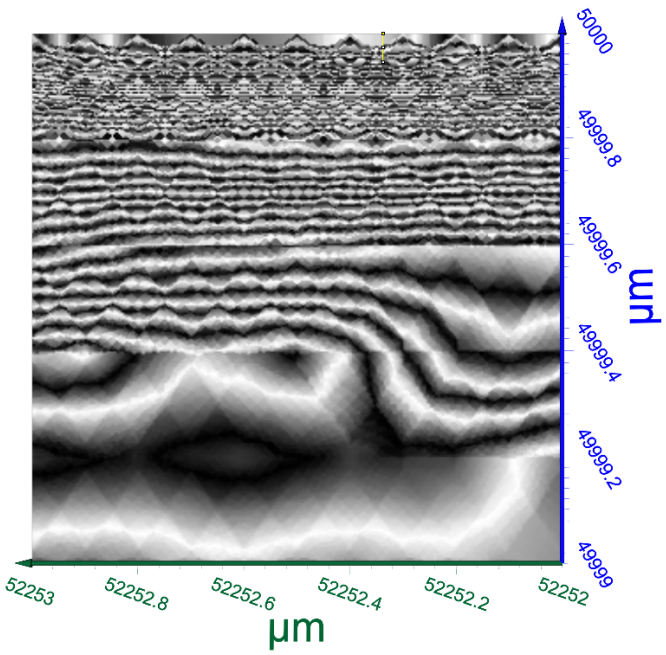

Fig. 10. Sample-D10: 1 μm^2 area (YZ surface) extracted from Fig. 9.

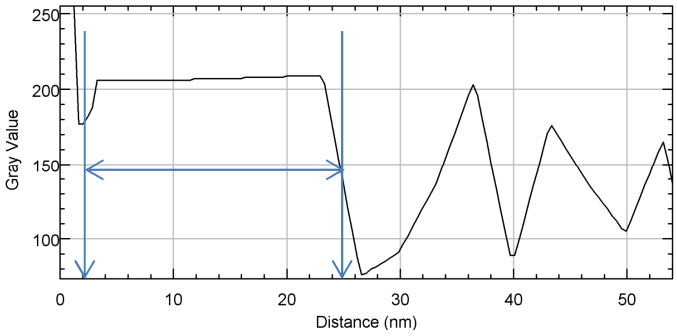

Fig. 11. Graphical analysis of sample-D10 from the image in Fig. 10. Measured thickness of the SiGe layer (top) is ~ 21 nm (see arrow).

IV. Conclusions

In this paper, 3D, sub-surface imaging is accomplished by means of terahertz multispectral reconstructive technique in a non-contact, non-destructive fashion with virtually no sample preparation requirements. A dendrimer dipole excitation based continuous wave terahertz source was used. Gridding with inverse distance to power equations was utilized for reconstructive imaging. Both 2D and 3D images were analyzed for unique quantification of layer thickness and lattice stacking faults. It was found that the techniques deployed herein are effective for visualizing the lattice structure from a 3D image of the samples. Details of stacking fault have been observed with quantitative lattice dimensions. Layer thicknesses of epitaxially grown SiGe layer on Ge buffer and also of Ge buffer on Si wafer match with the TEM results for the same sample. Sub-nanometer particulates were observed in the SiGe layer; the origin of which require further investigations. The non-contact measurement system outlined

here may be implemented for quality inspection at the production line as well as for various process development purposes.

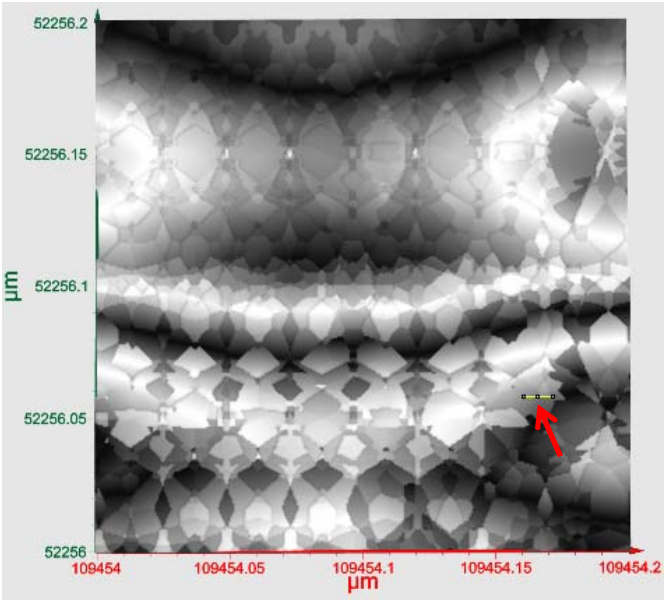

Fig. 12. Nanometer size particulate features visible in the SiGe layer of sample-D10. A single particle's (red arrow) size is analyzed in Fig. 13.

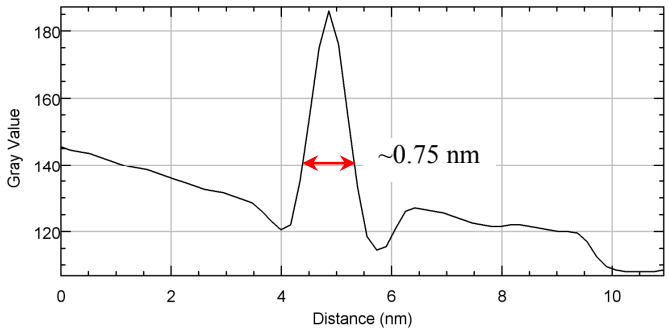

Fig. 13. Graphical analysis of a single particle indicates the smallest particles are less than a nanometer.

V. Appendix-I

Physical principles of reconstructive imaging: Terahertz multispectral reconstructive imaging and terahertz time-domain spectrometry for investigating different semiconductor wafers and nanomaterials was described elsewhere [3, 5]. Reconstructive imaging offers an important opportunity to define one's own pixel size (or voxel size in 3D) by a hardware and software combination. The procedure is outlined below.

A. Data structure: 3D imaging requires a value of a voxel, which is the smallest unit corresponding to a 3D space; i.e., $\{x, y, z, v\}$, where $\{x, y, z\}$ are the three orthogonal coordinates and v is the data at that point. To characterize a 3D space, data need to be generated for all over a given 3D volume. This is best done by an experimental scanning protocol where the volume is divided in to a number of slices (surfaces) and the slices are scanned one after another. Thus, the data are generated in the following sequence: for every $\{z_1, y_1\}$, a line is scanned giving $\{x_1,\ x_2 \ldots x_n\}$. Then the line is repeated for y_2 through y_n, while keeping the z_1 (i.e., the depth) fixed. This sequence of line at a given interval generated the first slice of the volume. Then the whole scan is repeated for z_2, yielding the second slice of the volume. This process is then repeated for all the slices to scan the whole volume. The line scan is done by a streaming data acquisition algorithm, where, a command is issued to move the scanner from the start point to the end point along the x-axis. As the positioning stage moves, its instantaneous position is recorded by the computer interface; thus generating the $\{x_1,\ x_2 \ldots x_n\}$ points for a given $\{z_i, y_j\}$. The reflected intensity or both the reflected and transmitted intensity is read simultaneously corresponding to each x_i. Once the whole volume is scanned, the data set is then used for generating the image via inverse distance to power equations.

B. Inverse distance to power equations: this is a method for grid-based map creation from measured $\{x, y, z, v\}$ data set. Practical $\{x, y, z\}$ based data typically comprise of irregularly spaced values; as such requires further computation to generate a grid-based map. The gridding process effectively interpolates data values for the lattice at locations where data values are absent. Therefore, closer the measured data points to each other, more accurate is the gridded image for feature sizes that are smaller than the hardware resolution. The current experimental setup has a hardware resolution of <25 nm. Therefore, the interpolation via inverse gridding method may be used to generate an image at 1 nm resolution or less. The reliability of the interpolation is tested by calibration with respect to known dimensions. A smoothing parameter may be applied during interpolation in order to suit the imaging requirements for a given specimen. The method does not extrapolate values beyond those found in the source data. The following equations are used for computation of the 3D lattice via inverse distance to a power [6, 7]:

$$\widehat{\boldsymbol{C}}_{\boldsymbol{j}} = \frac{\sum_{i=1}^{n} \frac{C_i}{h_{ij}^{\beta}}}{\sum_{i=1}^{n} \frac{1}{h_{ij}^{\beta}}} \qquad (1)$$

where, $h_{ij} = \sqrt{d_{ij}^2 + \delta^2}$,

h_{ij} is the effective separation distance between grid node "j" and the neighboring point "i";
$\widehat{\boldsymbol{C}}_{\boldsymbol{j}}$ are the interpolated values for lattice node "j";
C_i are the neighboring measured points;
d_{ij} is the distance between grid node "j" and the neighboring point "i";
β is the power or weighting parameter; and
δ is the smoothing parameter.

The power, β and the smoothing factor, δ, in the above computation may be chosen by the user to suit different imaging needs. Once the lattice is calculated, the surface image and volume image is generated by simply rendering the grid with a chosen color scheme. As an illustration of the functionality, consider a function, $f(x, y, z) = c * cos(x)$ to demonstrate the image formation. One can easily compute this

function over a given 3D space. Let us assume: $x \to 0 \ldots 2\pi, y \to 0 \ldots 6, z \to 0 \ldots 6$. Once the function is evaluated via the procedure described above, one can construct the data space. Then using the gridding method, one can reconstruct (map) the function over the given 3D space. The plot for the above function looks like as shown in Fig 14. Closer the grid points, smoother will be the surface. One can plot experimental data by the same procedure.

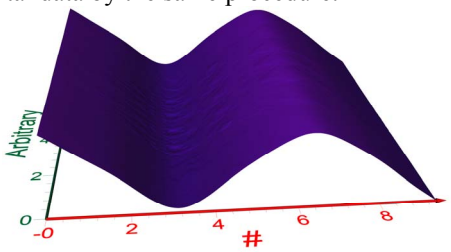

Fig. 14. 3D plot of the function f(x,y,z)=c*Cos(x).

Identifying the dislocations: Dislocations are identified primarily from lattice resolution images of a given specimen. It is important to identify the dislocations because they can strongly affect the local electronic and optical properties of semiconductors [12–14]. In an edge dislocation, localized lattice distortion exists along the end of an extra half-plane of atoms. A screw dislocation results from shear distortion. Many dislocations in crystalline materials have both edge and screws components; these are mixed dislocations. For edge dislocation line moves parallel to applied stress while for screw dislocation line moves perpendicular to applied stress. TEM tomography technique, for example, applies a 3D Fourier filtering [13] to enhance the contrast of the acquired images and help analyze crystallographic properties such as the dislocations.

Final remarks: As for the present article; the work described herein encompasses lattice imaging via terahertz multispectral technique. While stacking faults and dislocations are identified from the images, further work is being planned to illustrate the full capacity of the technique. However, it is difficult to find practical samples with known defects. More measurements are necessary encompassing different defect types. This will be attempted in future work.

VI. References

1. P.M. Mooney, "Strain relaxation and dislocations in SiGe/Si structures," IBM Research Division, T.J. Watson Research Center, PO Box 218, Yorktown Heights, NY 10598, USA, Materials Science and Engineering: R: Reports, Volume 17, Issue 3, 1 November 1996, Pages 105–146.
2. Anis Rahman and Aunik K Rahman, "Effective testing for wafer reject minimization by terahertz analysis and sub-surface imaging," ASMC 2014, Saratoga Springs, NY, 978-1-4799-3944-2/14/$31.00 ©2014 IEEE, pp. 151–155. http://arphotonics.net/ASMC2014_5.8.pdf
3. Rahman A, Rahman AK (2016), "Terahertz Spectroscopic Analysis and Multispectral Imaging of Epitaxially Grown Semiconductors with Nanometer Resolution." *J Biosens Bioelectron* 7: 229. DOI: 10.4172/2155-6210.1000229.
4. By personal correspondences with IMEC, TSMC Europe BV, Kapeldreef 75, 3001 Leuven, Belgium.
5. Anis Rahman, Aunik K Rahman, Takayuki Yamamoto, and Hiroshi Kitagawa, "Terahertz sub-nanometer sub-surface imaging of 2D materials," accepted for publication in the *Journal of Biosensors & Bioelectronics* (ISSN: 2155-6210).
6. Davis, John C. (1986) Statistics and Data Analysis in Geology. John Wiley and Sons, New York, NY.
7. Franke, R. (1982) Scattered Data Interpolation: Test of Some Methods, Mathematics of Computations, v. 33, n. 157, p. 181-200.
8. Fine, Morris E. (1921). "Introduction to Chemical and Structural Defects in Crystalline Solids", in Treatise on Solid State Chemistry Volume 1, Springer: New York.
9. Hirth, J. P. & Lothe, J. (1992). Theory of dislocations (2 ed.). Krieger Pub Co. ISBN 0-89464-617-6.
10. Gerald Burns, Solid State Physics, 1985, Academic Press: Orlando. ISBN-13: 978-0121460709
11. J. W. Matthews and A. E. Blakeslee, "Defects In Epitaxial Multilayers," *Journal of Crystal Growth*, 27 (1974) I 18-125.
12. D.J. Smith, "Chapter 1: Characterization of Nanomaterials Using Transmission Electron Microscopy," in Nanocharacterisation, 2nd Edition, Ed. A.I. Kirkland and S.I. Haigh, The Royal Society of Chemistry, Cambridge: 2015, ISBN: 978-1-84973-805-7.
13. C-C. Chen, C. Zhu, E.R. White, C-Y. Chiu, M.C. Scott, B.C. Regan, L.D. Marks, Y. Huang and J. Miao, "Three-dimensional imaging of dislocations in a nanoparticle at atomic resolution," Nature 496, 74–77 (04 April 2013) doi: 10.1038/nature12009.
14. D. Hull and D.J. Bacon, "Introduction to Dislocations," 5th Ed., Elsevier, Burlington: 2011. ISBN: 978-0-08-096672-4. CHAPTER 2: Observation of Dislocations.